Journal of Power Sources 271 (2014) 262–268

Contents lists available at ScienceDirect

Journal of Power Sources

journal homepage: www.elsevier.com/locate/jpowsour

An experimentally validated transient thermal model for cylindrical Li-ion cells

K. Shah [a], S.J. Drake [a], D.A. Wetz [b], J.K. Ostanek [c], S.P. Miller [c], J.M. Heinzel [c], A. Jain [a, *]

[a] Mechanical and Aerospace Engineering Department, University of Texas at Arlington, USA
[b] Electrical Engineering Department, University of Texas at Arlington, USA
[c] Naval Surface Warfare Center, Carderock Division, U.S. Navy, USA

HIGHLIGHTS

- Presents a transient thermal model for cylindrical Li-ion cells.
- Results are in excellent agreement with experimental data.
- Model helps understand transient thermal phenomena in Li-ion cells.
- Thermal performance during pulsed operation is analyzed.

ARTICLE INFO

Article history:
Received 29 May 2014
Received in revised form
11 July 2014
Accepted 18 July 2014
Available online 27 July 2014

Keywords:
Lithium-ion cells
Energy conversion
Transient thermal management
Battery cooling
Laplace transforms

ABSTRACT

Measurement and modeling of thermal phenomena in Li-ion cells is a critical research challenge that directly affects both performance and safety. Even though the operation of a Li-ion cell is in most cases a transient phenomenon, most available thermal models for Li-ion cells predict only steady-state temperature fields. This paper presents the derivation, experimental validation and application of an analytical model to predict the transient temperature field in a cylindrical Li-ion cell in response to time-varying heat generation within the cell. The derivation is based on Laplace transformation of governing energy equations, and accounts for anisotropic thermal conduction within the cell. Model predictions are in excellent agreement with experimental measurements on a thermal test cell. The effects of various thermophysical properties and parameters on transient thermal characteristics of the cell are analyzed. The effect of pulse width and cooling time for pulsed operation is quantified. The thermal response to multiple cycles of discharge and charge is computed, and cell-level trade-offs for this process are identified. The results presented in this paper may help understand thermal phenomena in Li-ion cells, and may contribute towards thermal design and optimization tools for energy conversion and storage systems based on Li-ion cells.

1. Introduction

Overheating and thermal runaway in Lithium-ion batteries is a significant technological challenge that has caused several well-documented incidents including fire in battery packs on aircraft [1]. Such incidents highlight safety challenges that may affect the adoption of Li-ion batteries in several applications with high C-rates, despite several other attractive features such as high energy density and specific energy [2,3]. The process of charging or discharging of a Li-ion cell inherently generates heat due to a number of well-known electrochemical and electrical mechanisms [4,5]. The temperature-sensitive nature of Li-ion cell technology makes it particularly prone to a self-sustained sequence of exothermic reactions once the temperature exceeds a certain threshold. Fundamentally, this process involves decomposition of the Solid-Electrolyte Inteface (SEI) [6,7], short circuit due to separator layer rupture from dendrite formation, etc., which ultimately leads to catastrophic failure [8]. This severely limits the use of Li-ion cell technology in several applications, particularly where high ambient temperature or high rates of cell discharge may be encountered.

The capability of accurate prediction of temperature fields within a cell is clearly of much technological importance. Such capability will help understand the close coupling between

* Corresponding author. 500 W First St, Rm 211, Arlington, TX 76019, USA. Tel.: +1 (817) 272 9338; fax: +1 (817) 272 2952.
E-mail address: jaina@uta.edu (A. Jain).

http://dx.doi.org/10.1016/j.jpowsour.2014.07.118
0378-7753/

electrochemical and thermal phenomena in the cell [4,5,9], and evaluate the effectiveness of candidate cooling technologies for thermal management of Li-ion cells [10,11]. However, despite the critical nature of thermal conduction in ensuring safety of Li-ion cells, only limited work exists on modeling of thermal transport within the cell [11,19]. Due to the spiral wound nature of the electrode stack, thermal conduction within the cell is expected to be highly anisotropic, which has been confirmed by recent measurements that report more than 100-fold difference between axial and radial thermal conductivity [13]. Some research has been reported on one-dimensional thermal models, including those that treat the entire cell as a lumped thermal mass [15,16]. Three-dimensional numerical simulations have also been presented [17]. System-level thermal simulations using finite-element tools have been presented [20,21]. Analytical expressions for the steady-state temperature field in a heat-generating Li-ion cell have been derived and validated with experimental data [12]. Results from this model show the strong dependence of temperature field on radial thermal conductivity and the nature of the convective boundary condition at the axial ends. In addition, this work also shows the existence of significant temperature gradients within the cell [12], due to which a lumped mass model may not appropriate for a Li-ion cell.

The operation of a Li-ion cell is inherently a transient thermal phenomenon. As a Li-ion cell is charged and discharged at a rate that changes with time based on variations in load requirements and power availability, the heat generation rate within a Li-ion cell also changes as a function of time. For example, sudden increase in power demand may produce pulsed spikes in the heat generation rate in the cell as a function of time, due to which the cell temperature may also rise. Depending on the thermal mass of the cell and the C-rate, a steady-state may never actually be reached, and the entire operation of the cell may be transient in nature. In such a case, it is important to predict the nature of temperature spikes in response to changes in C-rates, so that appropriate thermal management mechanisms may be designed. This highlights the need for a thorough fundamental understanding of transient thermal behavior of a Li-ion cell and the capability of prediction of temperature rise as a function of time due to time-varying heat generation rate.

Most research reported on modeling of thermal transport in Li-ion cells only predicts steady state temperature distribution [12]. Given the inherently transient nature of the operation of a Li-ion cell, development of transient thermal models in highly desirable. Such a capability is expected to result in design rules for run-time thermal behavior of Li-ion cells. For example, it would be of interest to determine the expected temperature excursion for a given increase in heat generation rate due to a short-time spike in power flow into or out of the cell. Such design rules are expected to contribute towards enhanced safety of Li-ion cells, and in resolving system-level multi-disciplinary optimization problems, such as the optimization between total discharge time and maximum temperature reached.

This paper describes an analytical solution to the energy conservation equations that govern transient thermal transport within a heat-generating cylindrical Li-ion cell. This approach results in expressions for the temperature field in the cell due to time-varying heat generation rate. Results are shown to be in good agreement with experimental data on a thermal test cell. The experimentally-validated analytical model is used to develop an understanding of the role of various physical parameters on transient temperature rise. The thermal response of the cell to a spike in heat generation, and to a sequence of multiple discharge-charge cycles is also investigated. Various trade-offs between thermal design and other cell-level design considerations are identified.

The next section outlines the transient governing energy equations and presents their solution for time-varying transient heat generation rate in the cell. Section 3 discusses experimental validation of the analytical model. Section 4 discusses applications of the analytical model in order to develop an understanding of the transient thermal phenomena that occur in a Li-ion cell and their dependence on various physical parameters.

2. Analytical model

Fig. 1 shows a schematic of a heat-generating, cylindrical Li-ion cell of radius R and height H. Heat generation within the cell occurs due to a variety of physical mechanisms, including Joule heating, entropic heating, enthalpies of reactions, etc. [4,5]. The volumetric heat generation rate $Q(t)$ is assumed to be uniform in space, but time-dependent. Convective heat transfer is assumed to occur on the outside surfaces, with heat transfer coefficients given by h_r and h_z for the radial and axial outer surfaces respectively. Thermal conductivity of the Li-ion cell is assumed to be anisotropic [13], with values of k_r and k_z in radial and axial directions respectively.

The transient temperature field for this problem is governed by the following energy conservation equation:

$$\frac{k_r}{r}\frac{\partial}{\partial r}\left(r\frac{\partial\theta}{\partial r}\right)+k_z\frac{\partial^2\theta}{\partial z^2}+Q(t)=\rho C_p\frac{\partial\theta}{\partial t} \tag{1}$$

where $\theta(r,z,t)$ is the temperature rise above ambient.

Equation (1) is a non-homogeneous, transient partial differential equation subject to four homogeneous boundary conditions given by

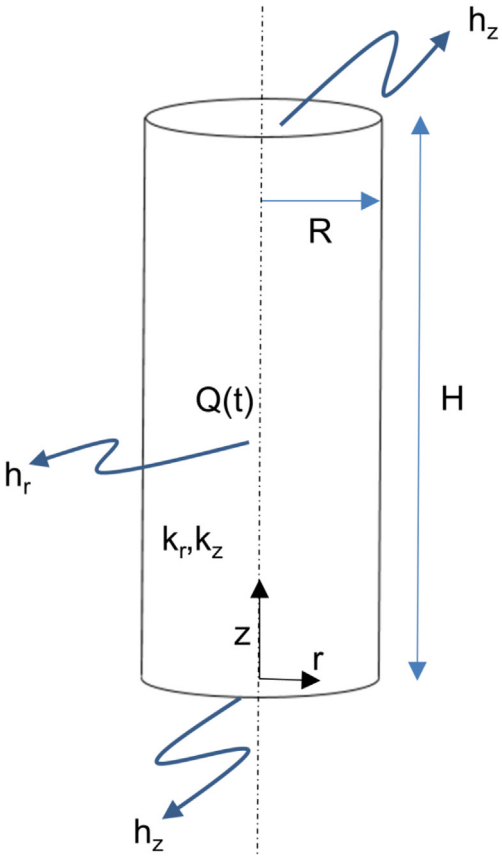

Fig. 1. Schematic of the geometry of a cylindrical Li-ion cell under consideration.

$$\frac{\partial\theta}{\partial z} = \frac{h_z}{k_z}\theta \quad \text{at } z = 0 \tag{2}$$

$$\frac{\partial\theta}{\partial z} = -\frac{h_z}{k_z}\theta \quad \text{at } z = H \tag{3}$$

$$\frac{\partial\theta}{\partial r} = 0 \quad \text{at } r = 0 \tag{4}$$

$$\frac{\partial\theta}{\partial z} = -\frac{h_r}{k_r}\theta \quad \text{at } r = R \tag{5}$$

In addition, it is assumed that the cell is at ambient temperature at $t = 0$

$$\theta = 0 \quad \text{at } t = 0 \tag{6}$$

Deriving an analytical solution for Equation (1) subject to boundary conditions (2)–(5), and initial condition (6) is not straightforward due to the time-dependence of the heat generation term. If this term were invariant with time, the problem could be solved easily by splitting the solution into two components, absorbing Q in the first component, and using a separation of variables approach for the second component [22,23]. In this general case, however, the time dependence of $Q(t)$ requires that the solution be derived using other methods, such as Laplace transforms. To do so, Laplace transform of Equations (1)–(5) is carried out, resulting in the following governing equation in the Laplace space:

$$\frac{k_r}{r}\frac{\partial}{\partial r}\left(r\frac{\partial\overline{\theta}}{\partial r}\right) + k_z\frac{\partial^2\overline{\theta}}{\partial z^2} + \overline{Q}(s) = \frac{\rho C_p}{s}\overline{\theta} \tag{7}$$

subject to

$$\frac{\partial\overline{\theta}}{\partial z} = \frac{h_z}{k_z}\overline{\theta} \quad \text{at } z = 0 \tag{8}$$

$$\frac{\partial\overline{\theta}}{\partial z} = -\frac{h_z}{k_z}\overline{\theta} \quad \text{at } z = H \tag{9}$$

$$\frac{\partial\overline{\theta}}{\partial r} = 0 \quad \text{at } r = 0 \tag{10}$$

$$\frac{\partial\overline{\theta}}{\partial r} = -\frac{h_r}{k_r}\overline{\theta} \quad \text{at } r = R \tag{11}$$

where $\overline{\theta}(r,z)$ and $\overline{Q}(s)$ are Laplace transforms of the temperature rise field $\theta(r,z,t)$ and heat generation term $Q(t)$ respectively. s is the Laplace variable.

The governing energy equation in Laplace space is more amenable to a solution since it does not involve transient terms. The solution is determined by first splitting $\overline{\theta}(r,z)$ into an axially varying component governed by an ordinary differential equation, and the remainder, which is governed by a homogeneous partial differential equation. The final solution is found to be

$$\overline{\theta}(r,z) = \overline{p}(z) + \sum_{n=1}^{\infty} c_n I_0(\lambda_n r)[\mu_n H\cos(\mu_n z) + Bi_H \sin(\mu_n z)] \tag{12}$$

where,

$$\overline{p}(z) = A\cdot\sinh\left(\sqrt{\frac{\rho C_p s}{k_z}}z\right) + B\cdot\cosh\left(\sqrt{\frac{\rho C_p s}{k_z}}z\right) \tag{13}$$

The coefficients A and B in Equation (13) are determined by using boundary conditions in the z-direction, which results in

$$A = \frac{\frac{\overline{Q}(s)}{\rho C_p s}\left(\sqrt{\rho C_p s k_z}\sinh\left(\sqrt{\frac{\rho C_p s}{k_z}}H\right) + h_z\left(\cosh\left(\sqrt{\frac{\rho C_p s}{k_z}}H\right) - 1\right)\right)}{2\sqrt{\rho C_p s k_z}\cosh\left(\sqrt{\frac{\rho C_p s}{k_z}}H\right) + h_z\sinh\left(\sqrt{\frac{\rho C_p s}{k_z}}H\right) + \frac{\rho C_p s k_z}{h_z}\sinh\left(\sqrt{\frac{\rho C_p s}{k_z}}H\right)} \tag{14}$$

$$B = \frac{A\sqrt{\rho C_p s k_z}}{h_z} - \frac{\overline{Q}(s)}{\rho C_p s} \tag{15}$$

Note that the series coefficients c_n in Equation (12) are given by

$$c_n = \frac{-Bi_R\cdot\frac{1}{H}\int_0^H \overline{p}(z)[\mu_n H\cos(\mu_n z) + Bi_H\sin(\mu_n z)]dz}{\frac{1}{2}\left[(\mu_n H)^2 + Bi_H^2 + 2Bi_H\right]\cdot\left[\lambda_n R\cdot I_0'(\lambda_n R) + Bi_R I_0(\lambda_n R)\right]} \tag{16}$$

The eigenvalues μ_n are obtained from roots of the transcendental equation

$$\tan(\mu H) = \frac{2Bi_H\cdot(\mu H)}{(\mu H)^2 - Bi_H^2} \tag{17}$$

where Bi_H and Bi_R are axial and radial Biot numbers [24], respectively, defined as $Bi_H = h_z H/k_z$ and $Bi_R = h_r R/k_r$.

Finally

$$\lambda_n = \sqrt{\gamma\left(\frac{\rho C_p s}{k_z} + \mu_n^2\right)} \tag{18}$$

where γ is the degree of anisotropy given by

$$\gamma = \frac{k_z}{k_r} \tag{19}$$

Equations (12)–(19) represent an analytical solution for the temperature field in the Laplace space. Since the resulting expression is somewhat complicated, conversion into time domain is carried out using de Hoog's quotient difference algorithm [25] for inverse Laplace transformation, as implemented by Hollenbeck [26].

While the solution methodology described above is applicable for spatially-uniform heat generation rate, a different approach needs to be adopted if, in addition to time, heat generation rate is a function of space as well. This could be done similar to a recently reported approach for solving the corresponding steady state problem with space dependent heat generation [12]. For example, if

Q is a function of z and t, the forcing function in the governing equation in Laplace space $\overline{Q}(z,s)$ will have a z-dependence. In order to derive a solution for this case, $\overline{Q}(z,s)$ is expressed as a polynomial expansion [27], following which the function $\overline{p}(z)$ can be obtained through integration of the polynomial terms. Once $\overline{p}(z)$ is known, determination of the remainder of the solution is similar to the procedure described above. For further details, the reader is referred to the recently reported solution of the steady-state problem using this approach [12].

3. Experimental validation

A thermal test cell is utilized for experimentally validating the thermal model presented in Section 2. This thermal test cell has the same dimensions as a 26650 cell, and has a thin stainless steel resistive heater rolled inside the cell body. The advantage of this test cell over an actual 26650 cell is that the heat generation rate in the test cell can be precisely controlled by changing the amount of electric current passing through the resistive heater. In comparison, it is difficult to obtain a specific heat generation rate in an actual Li-ion cell, since the heat generation rate is known to vary with time, even for constant current charge or discharge processes [5]. Since the objective here is to validate an analytical model with a known heat generation rate, the thermal test cell is preferred over an actual 26650 cell.

The test cell is placed in a chamber without forced air flow, representative of natural convection conditions. A K-type thermocouple attached to the outside surface of the test cell at mid-height provides temperature measurements as a function of time, which is compared against computations based on the model shown in Section 2. A picture of the thermal test cell with the thermocouple and lead wires for the heater is shown in the inset of Fig. 2. A Keithley 2401 sourcemeter is used to source the heating current, and a NI 9213 DAQ is used for temperature acquisition. All instruments are controlled by a LabVIEW code, which regularly makes minor adjustments to the heating current in order to provide constant power. This accounts for any increase in electrical resistance of the heater due to increased temperature inside the cell.

The analytical model in Section 2 is used to predict the temperature as a function of time for the experimental conditions. Thermal properties of the same test cell used in experiments are implemented in the model. These properties – radial and axial thermal conductivities and heat capacity – are determined by using a recently described experimental technique [13]. In this method, external heat flux is applied on an insulated cell is either radial or axial direction. The thermal response of the cell measured at a specific location is compared against an analytical model to determine the radial and axial thermal conductivities as well as heat capacity of the cell. The measured values for the test cell are found to be close to recently reported values for an actual 26650 cell. The convective heat transfer coefficients h_r and h_z are assumed to be 10 W m^{-2} K^{-1}, which is representative of natural convection cooling [24]. As recently reported [12], a similar value of h_r and h_z has been shown to result in excellent agreement between experimental data and an analytical model for steady-state thermal conditions.

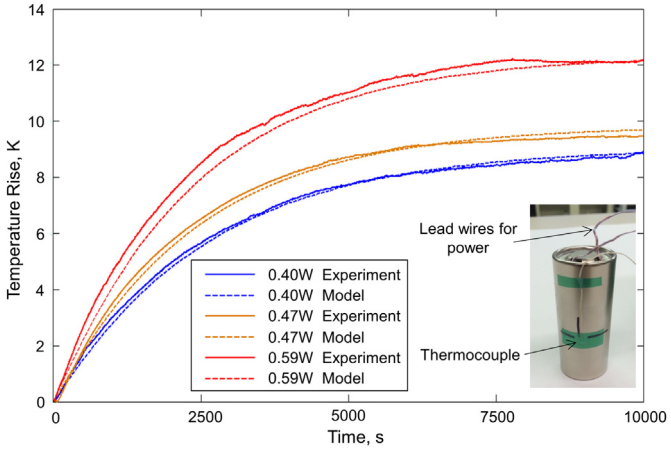

Fig. 2. Temperature plot showing experimental validation of the analytical model.

Fig. 2 presents the measured temperature rise at the outer surface at mid-height ($r = R, z = H/2$) as a function of time for three different heat generation rates. The temperature variation predicted by the analytical model presented in Section 2 is also shown in Fig. 2. In each case, the analytical model is in excellent agreement with experimental data. The model correctly captures both absolute temperature rise and the time scale for the temperature rise for each power. The maximum deviation between the two during the entire experiment is 0.63 °C.

4. Results and discussion

For further confirmation of the validity and accuracy of the analytical model derived in Section 2, the temperature field is computed as a function of time for two cases, and compared with results from finite-element simulations. These cases address the temperature response of a 26650 Li-ion cell to two different heating profiles – a constant heating of 6 W, and a step function where the heating power spikes from 2 W to 10 W between $t = 1000$ s and $t = 1500$ s.

Note that the heat generation rate is closely related to the C-rate through the discharge current and effective internal resistance of the cell as follows:

$$Q = I^2 \cdot r_{\text{int}} \tag{20}$$

Thus, assuming a 2.6 A-hr cell with an effective internal resistance of 20 mΩ, the 6 W heating case corresponds to a C-rate of 6.7C and the 2–10 W range corresponds to a C-rate range of 3.8–8.6C.

Fig. 3(a) and (b) plots the temperature profile computed for these cases using the analytical model, along with results from finite-element simulations. Adequately fine meshing is carried out in these simulations to ensure grid-independence of results. In both cases, there is excellent agreement between the analytical model and results from finite-element simulations, which provides additional validation of the analytical model presented in Section 2.

Since the external heat transfer coefficient h_r and radial thermal conductivity k_r are key parameters that determine thermal performance of the Li-ion cell, temperature is computed as a function of time for different values of these parameters, while considering the same heat generation rate. These plots, presented in Fig. 4(a) and (b) show that the temperature profile and the peak temperature are strong functions of both h_r and k_r. The cell temperature reduces as h_r increases, since greater convective heat transfer on the cell surface reduces heat accumulated within the cell, and hence the cell temperature. However, the effect of increasing h_r on lowering the cell temperature saturates, as seen in Fig. 4(a). Increasing the value of h_r beyond around 500 W m^{-2} K^{-1} has negligible incremental effect on reducing the cell temperature. This can be explained in terms of the overall thermal resistance comprising of the thermal conduction resistance within the cell, and convective resistance from the cell surface to the ambient. Once the latter resistance has been reduced sufficiently, it does not dominate any more, and the cell temperature becomes nearly

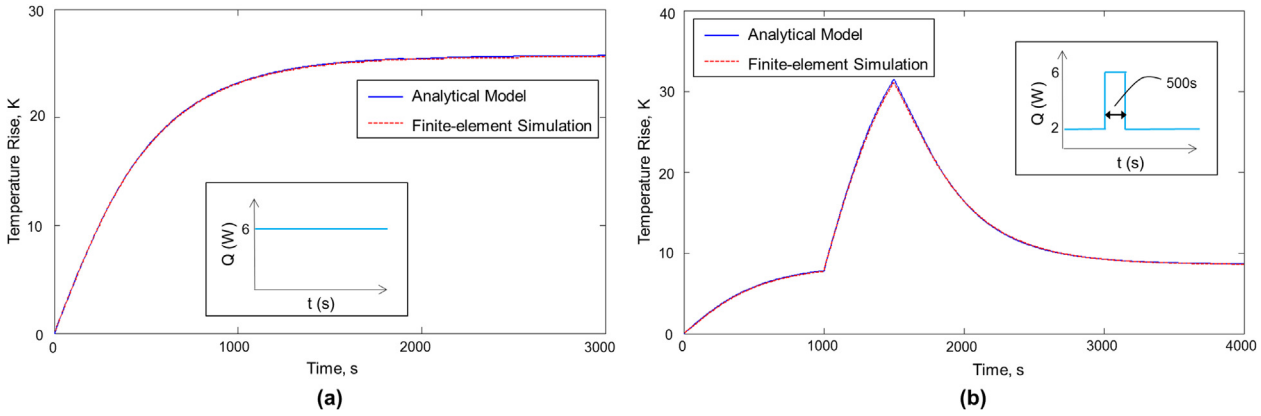

Fig. 3. Comparison of analytical model with finite-element simulations (a) constant, and (b) pulsed heat generation profiles.

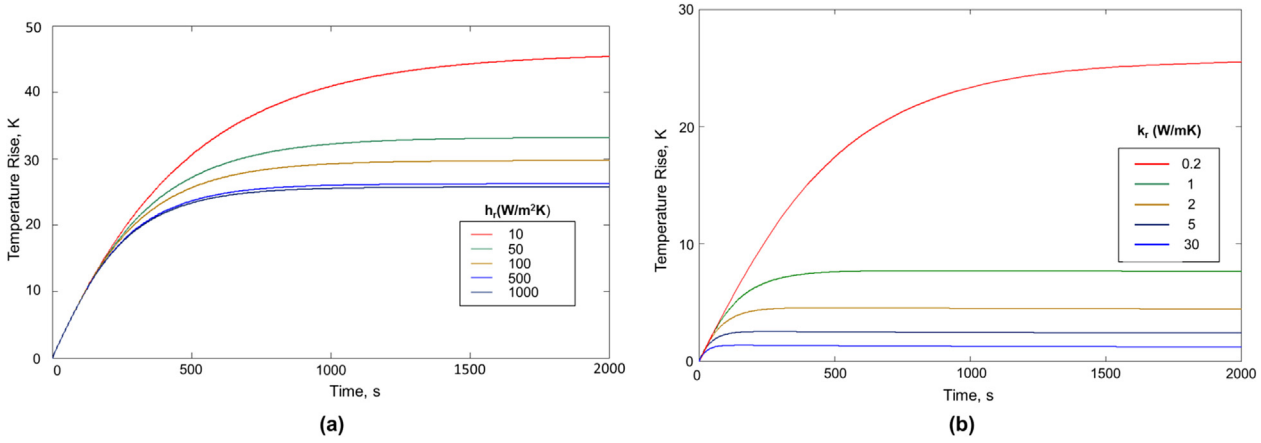

Fig. 4. Plots showing variation in temperature profiles as function of (a) convective heat transfer coefficient, h_r, (b) radial thermal conductivity, k_r.

independent of the convective thermal resistance. On the other hand, increasing the value of k_r, which contributes towards reducing the internal conduction resistance, is found to strongly reduce the cell temperature, as shown in Fig. 4(b). No saturation effect similar to Fig. 4(a) is observed in this case. The temperature curve continues to drop with increasing k_r. Note that the largest value of k_r examined in Fig. 4(b) is 30 W $m^{-1}K^{-1}$, which is the experimentally measured axial thermal conductivity [13], and hence likely to be the upper limit of k_r.

The analytical model is also used to investigate the thermal effect of transient spikes in heat generation rate during the operation of a Li-ion cell. It is assumed that the Li-ion cell encounters a pulse of excess load resulting in a 13.5 W heat generation, corresponding to 10C discharge rate. This is followed by zero heat generation rate. Such a pulse can occur, for example, during sudden acceleration of a hybrid/electric vehicle that demands large power draw from the battery for a short amount of time [28]. It is clearly of much importance to understand the thermal phenomena associated with such a power draw, particularly the peak temperature reached by the cell, and the time taken by the cell to recover to baseline temperature after the power draw ends. Fig. 5 presents plots of the cell temperature as a function of time for different pulse widths in the 5–100 s range, which may be typical for vehicular applications [28]. h_r and h_z are assumed to be 100 W m^{-2} K^{-1} each, and k_r and k_z are assumed to be 0.2 and 30 W m^{-1} K^{-1} respectively, based on measurements [13]. Fig. 5 shows that as the pulse width increases, the cell temperature increases as expected. The time taken to cool down back to a specific temperature also increases as the pulse width increases. One possible strategy for timely cooling is to increase convective heat transfer during the cooling process, for example by blowing more air or coolant, which effectively increases the value of h_r. Fig. 6 plots the time required by the cell to cool down to a temperature of 1 °C above baseline temperature after a 50 s pulse of 13.5 W as a function of the convective heat

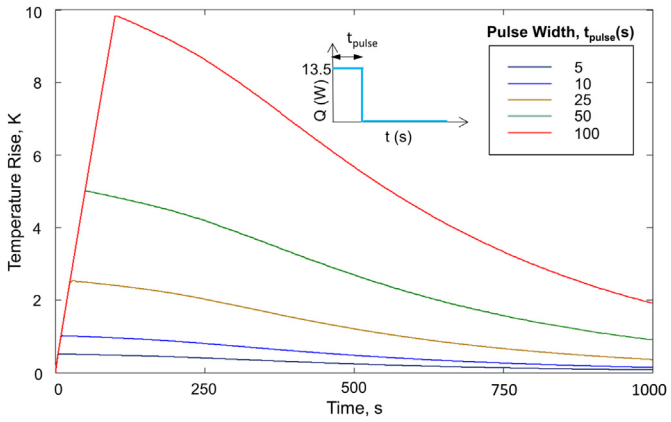

Fig. 5. Plot of the maximum cell temperature as a function of time for different pulse widths.

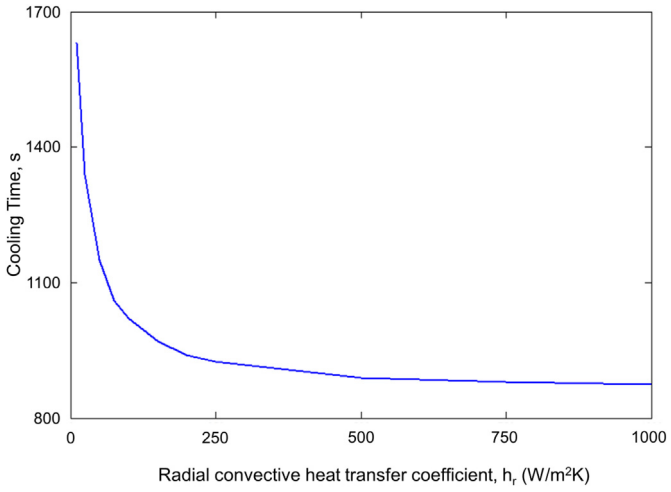

Fig. 6. Plot of cooling time required to cool down to a baseline temperature of 1 °C above ambient as a function of the convective heat transfer coefficient h_r.

transfer coefficient h_r. In general, the time required to cool reduces as h_r increases. However, this effect saturates, similar to the saturation observed in Fig. 4(a), wherein beyond around 500 W m^{-2} K^{-1}, increasing h_r further results in only minimal improvement in time needed to cool. As shown in Fig. 4(b), further improvements in the thermal performance of the Li-ion cell must come from improved thermal conductance within the cell due to dominance of the internal conduction resistance in overall thermal resistance.

Another pulsed power scenario with interesting and technologically relevant thermal concerns is the discharge of a amount of energy in a pulse. In case the cell is to discharge a specific amount of energy, there may be a fundamental choice in whether to discharge the energy at high power over a short time, or at low power over a large time. While the former choice increases the power dissipated in the cell, there is more time in the latter for the cell temperature to rise. This problem is examined using the analytical model presented in Section 2. In particular, the maximum cell temperature is plotted in Fig. 7(a) and (b) as a function of time for a number of discharges that each dissipate a fixed amount of energy, but at different powers and discharge times. Fig. 7(a) addresses relatively shorter pulse widths, with total 60 J energy dissipation, while Fig. 7(b) addresses longer pulse widths, with total 600 J dissipation. h_r, h_z, k_r and k_z are assumed to be the same as in Fig. 5. . Fig. 7(a) shows that at low pulse widths, the peak temperature reached is not a strong function of pulse width. On the other hand, for larger pulse durations, as shown in Fig. 7(b), the cell temperature increases with decreasing discharge time due to increased power. Thus, it may be preferable to discharge over a longer time with lower power, although this effect is not significant in the short pulse width range.

Several energy conversion applications may require multiple periodic discharges – each of which result in heat generation – from the Li-ion cell, with a cooling time interspersed between successive discharges. Such successive discharges may cause heat buildup within the cell and excessive temperature rise, possibly leading to thermal runaway. As a result, thermal analysis of a multiple discharge process is of critical importance. The model presented in Section 2 is utilized to compute the temperature as a function of time for a 10-step process of successive discharges. Each discharge is assumed to result in 6 W heat generation over a 10 s period. Fig. 8(a) presents the resulting temperature curves for two cooling times of 10 and 20 s. The cooling time is a critical parameter in the thermal well-being of the cell during the multiple discharge process. Fig. 8(b) plots the peak temperature rise at the end of the ten-cycle process as a function of cooling time between successive discharges. A large cooling time permits the cell to recover between discharges, whereas heat buildup may occur within the cell if the cooling time is too small. Increasing the cooling time – which is clearly thermally beneficial – however, is in conflict with possible system-level goals of reducing total energy conversion time. A careful balance between conflicting objectives, driven by analytical models such as ones presented here may be the key for safe and optimal operation of Li-ion cell based energy conversion systems.

5. Conclusions

It is important to fully understand thermal characteristics of a Li-ion cell in response to time-varying heat generation rate that are likely to be encountered in practical applications for energy storage and conversion. This paper contributes in this important direction by developing an experimentally-validated model to predict transient temperature fields in a Li-ion cell. Following model validation using experimental data obtained on a thermal test cell, the model is utilized to understand the effect of various thermal parameters on temperature distribution in the cell. The thermal response to

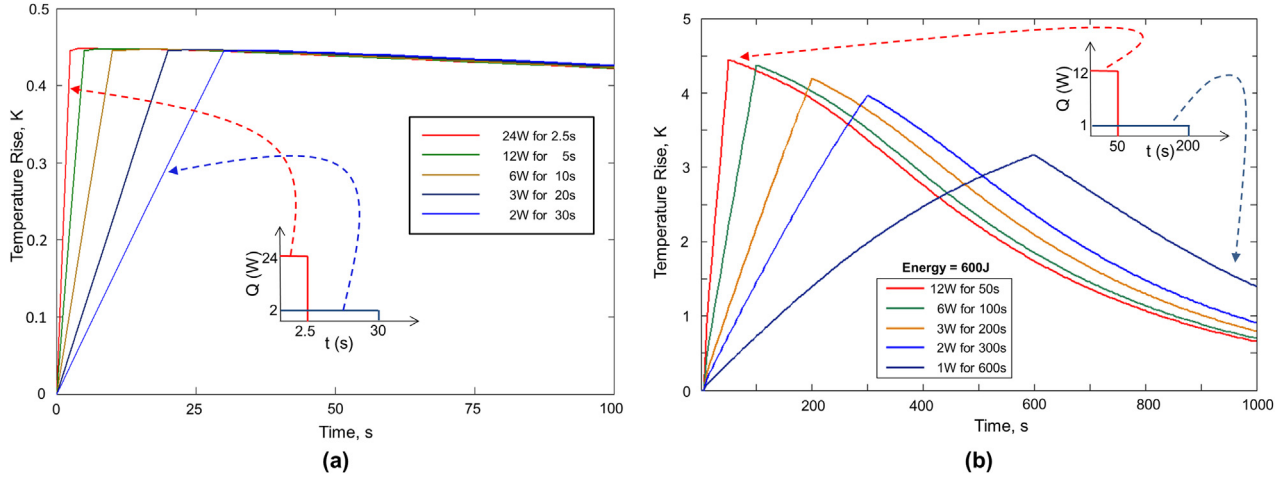

Fig. 7. Temperature profile for various discharge rates dissipating a constant total energy for (a) short pulse duration, and (b) long pulse duration.

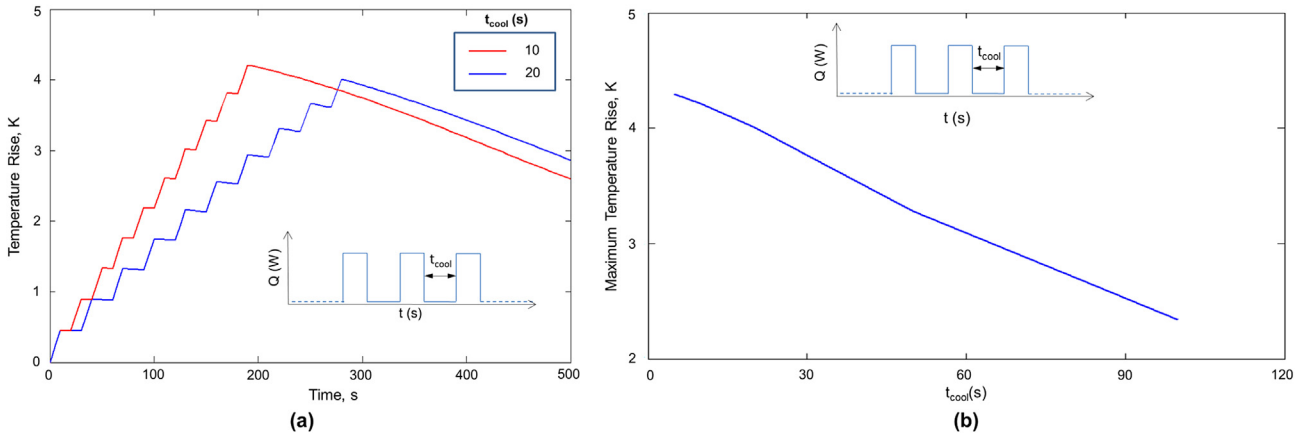

Fig. 8. (a) Comparison of temperature profile for two different ten-step discharge–charge processes with cooling times of 10 s and 20 s, (b) Plot showing dependence of maximum temperature rise on cooling time.

pulsed heating in a cell is studied. These results may be helpful in designing effective thermal management tools for a Li-ion cell, and in ensuring safe and optimal operation of a Li-ion cell.

Acknowledgments

This research was partly under ONR grant number N000141310819. The authors acknowledge assistance from Mr. Jared Jones in automation of data acquisition for the experiments.

References

[1] D. Lisbona, T. Snee, Process Saf. Env. Prot. 89 (2011) 434–442.
[2] M. Armand, J.-M. Tarascon, Nature 451 (2008) 652–657.
[3] B. Scrosati, J. Garche, J. Power Sources 9 (2010) 2419–2430.
[4] D. Bernardi, E. Pawlikowski, J. Newman, J. Electrochem. Soc. 132 (1985) 5.
[5] C.R. Pals, J. Newman, J. Electrochem. Soc. 142 (1995) 3274.
[6] A. Du Pasquier, F. Disma, T. Bowmer, A.S. Gozdz, G. Amatucci, J.M. Tarascon, J. Electrochem. Soc. 145 (1998) 472.
[7] H. Maleki, G. Deng, A. Anani, J. Howard, J. Electrochem. Soc. 146 (1999) 3224–3229.
[8] G.-H. Kim, A. Pesaran, R. Spotnitz, J. Power Sources 170 (2007) 476–489.
[9] A.A. Pesaran, M. Keyser, in: Proc. Ann. Battery Conf., 2001.
[10] R. Sabbah, R. Kizilel, J.R. Selman, S. Al-Hallaj, J. Power Sources 182 (2008) 630–638.
[11] T. Bandhauer, S. Garimella, Appl. Therm. Eng 61 (2013) 756–769.
[12] K. Shah, S.J. Drake, D.A. Wetz, J.K. Ostanek, S.P. Miller, J.M. Heinzel, A. Jain, J. Power Sources 258 (2014) 374–381.
[13] S.J. Drake, D.A. Wetz, J.K. Ostanek, S.P. Miller, J.M. Heinzel, A. Jain, J. Power Sources 252 (2014) 298–304.
[14] S.C. Chen, C.C. Wan, Y.Y. Wang, J. Power Sources 140 (2005) 111–124.
[15] W. Fang, O.J. Kwon, C.-Y. Wang, Int. J. Energy Res. 34 (2010) 107–115.
[16] C. Forgez, D.V. Do, G. Friedrich, M. Morcrette, C. Delacourt, J. Power Sources 195 (2010) 2961–2968.
[17] Y. Chen, J.W. Evans, J. Electrochem. Soc. 140 (1993) 1833–1838.
[18] P. Taheri, M. Yazdanpour, M. Bahrami, J. Power Sources 243 (2013) 280–289.
[19] Q. Wang, P. Ping, X. Zhao, G. Chu, J. Sun, C. Chen, J. Power Sources 208 (2012) 210–224.
[20] G. Karimi, X. Li, Int. J. Energy Res. 37 (2012) 13–24.
[21] A. Mills, S. Al-Hallaj, J. Power Sources 41 (2005) 307–315.
[22] N. Ozisik, Heat Conduction, second ed., John Wiley & Sons, 1993.
[23] H.S. Carslaw, J.C. Jaegar, Conduction of Heat in Solids, second ed., Clarendon Press, 1959.
[24] F.P. Incropera, D.P. Dewitt, Introduction to Heat Transfer, third. ed., Wiley Inc., 2006.
[25] F.R. de Hoog, J.H. Knight, A.N. Stokes, SIAM J. Sci. Stat. Comput. 3 (1982) 357–366.
[26] K.J. Hollenbeck, INVLAP.M: A Matlab Function for Numerical Inversion of Laplace Transforms by the de Hoog Algorithm, 1998 available at: http://www.isva.dtu.dk/staff/karl/invlap.htm (accessed 01.01.12).
[27] E. Kreyszig, Advanced Engineering Mathematics, tenth ed., Wiley Inc., 2011.
[28] M. Ceraolo, G. Lutzemberger, M. Marracci, High power lithium batteries usage in hybrid vehicles, in: Vehicle Power and Propulsion Conference (VPPC), 2010.